iScience, Volume *27*

Supplemental information

Monitoring GPCR conformation with GFP-inspired dyes

Anatoliy Belousov, Ivan Maslov, Philipp Orekhov, Polina Khorn, Pavel Kuzmichev, Nadezhda Baleeva, Vladislav Motov, Andrey Bogorodskiy, Svetlana Krasnova, Konstantin Mineev, Dmitry Zinchenko, Evgeni Zernii, Valentin Ivanovich, Sergei Permyakov, Johan Hofkens, Jelle Hendrix, Vadim Cherezov, Thomas Gensch, Alexander Mishin, Mikhail Baranov, Alexey Mishin, and Valentin Borshchevskiy

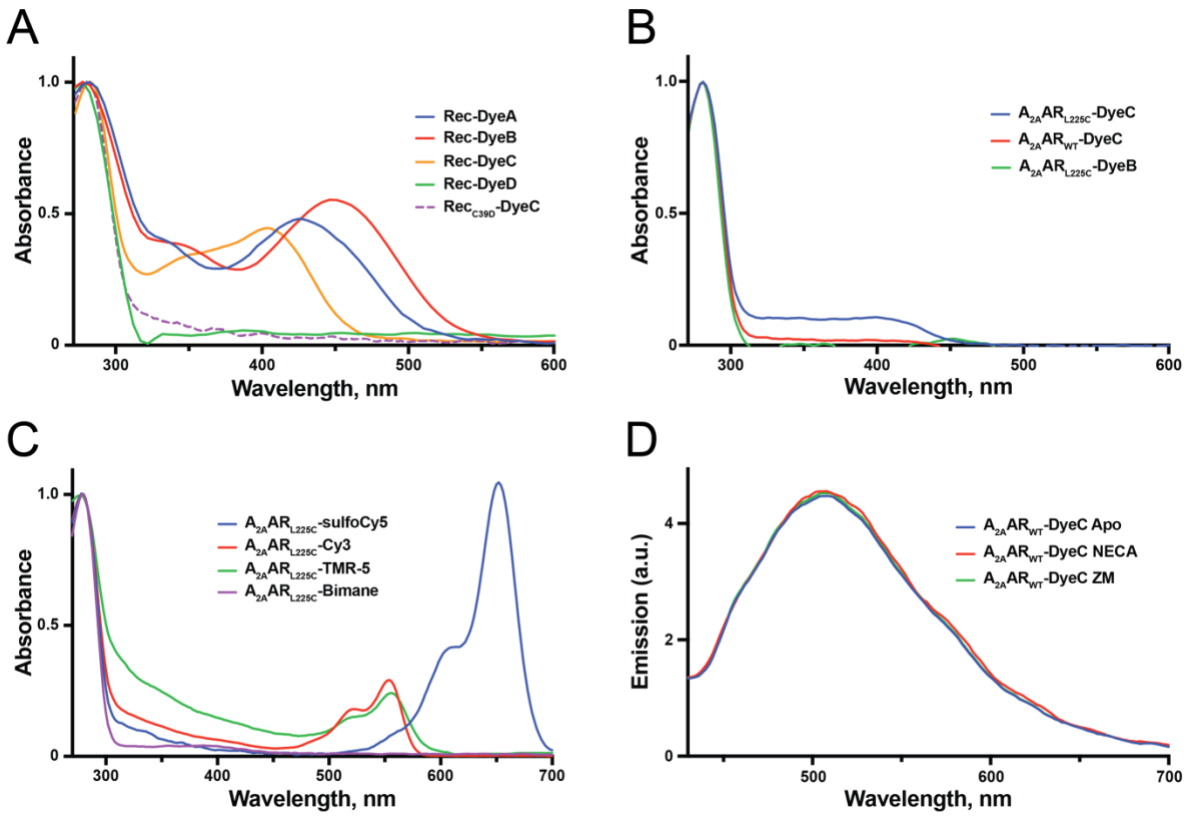

Figure S1. Absorbance spectra of labeled Rec and $A_{2A}AR$, and fluorescence emission spectra of $A_{2A}AR_{WT}$ labeled with DyeC, related to Figures 2-3.
A: Absorbance spectra of Rec labeled with synthesized GFP-inspired fluorophores. Rec$_{C39D}$-DyeC is used as a control for labeling specificity. Labeling efficiencies are ~ 90 %, 100 %, 85 %, and <5 % for Rec with DyeA, DyeB, DyeC, and DyeD, respectively, and <5 % for Rec$_{C39D}$. **B:** Absorbance spectra of $A_{2A}AR_{L225C}$ labeled with DyeC and DyeB. $A_{2A}AR_{WT}$-DyeC is used as a control for labeling specificity. Labeling efficiencies are <5 % and ~ 80 % for $A_{2A}AR_{L225C}$ with DyeB and DyeC, respectively, and <10 % for $A_{2A}AR_{WT}$-DyeC. **C:** Absorbance spectra of $A_{2A}AR_{L225C}$ labeled with sulfo-Cy5, Cy3, TMR-5, and Bimane. Labeling efficiencies are ~40%, ~25%, ~30%, and ~66% for $A_{2A}AR_{L225C}$ with sulfo-Cy5, Cy3, TMR-5, and Bimane, respectively. The absorption spectra **A, B, C** are normalized by the protein absorption maximum (280 nm). **D:** Fluorescence emission spectra of $A_{2A}AR_{WT}$-DyeC with added ligands. $A_{2A}AR_{WT}$-DyeC shows no response to the agonist NECA as opposed to $A_{2A}AR_{L225C}$-DyeC. This result suggests that there is no contribution to the change in $A_{2A}AR_{L225C}$-DyeC emission from nonspecific labeling. Excitation wavelength was 410 nm.

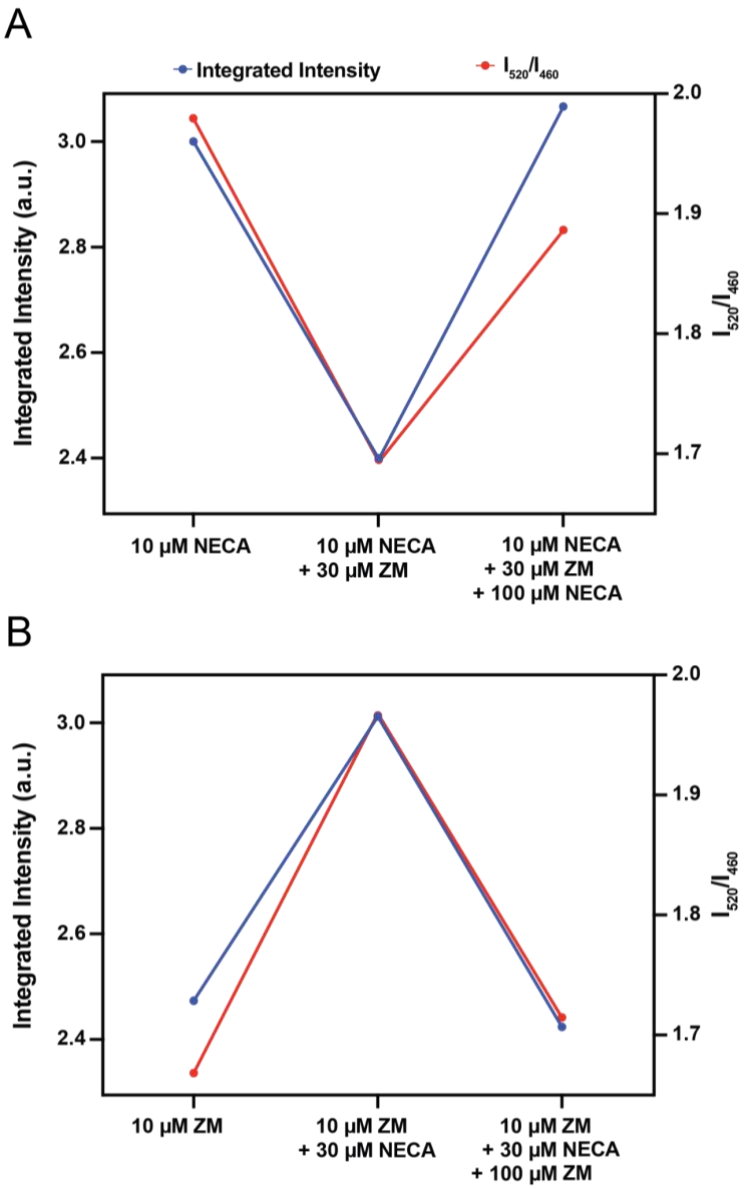

Figure S2. Displacement of ligands in $A_{2A}AR_{L225C}$-DyeC, related to Figure 3.
Two experiments were performed. In the first experiment (**A**), 10 µM NECA was added initially, followed by the addition of 30 µM ZM241385, and finally NECA was added again to a final concentration of 110 µM. In the second experiment (**B**), 10 µM ZM241385 was added initially, followed by the addition of 30 µM NECA, and finally ZM241385 was added again to a final concentration of 110 µM. Protein concentration was 2 µM. Excitation wavelength was 410 nm.

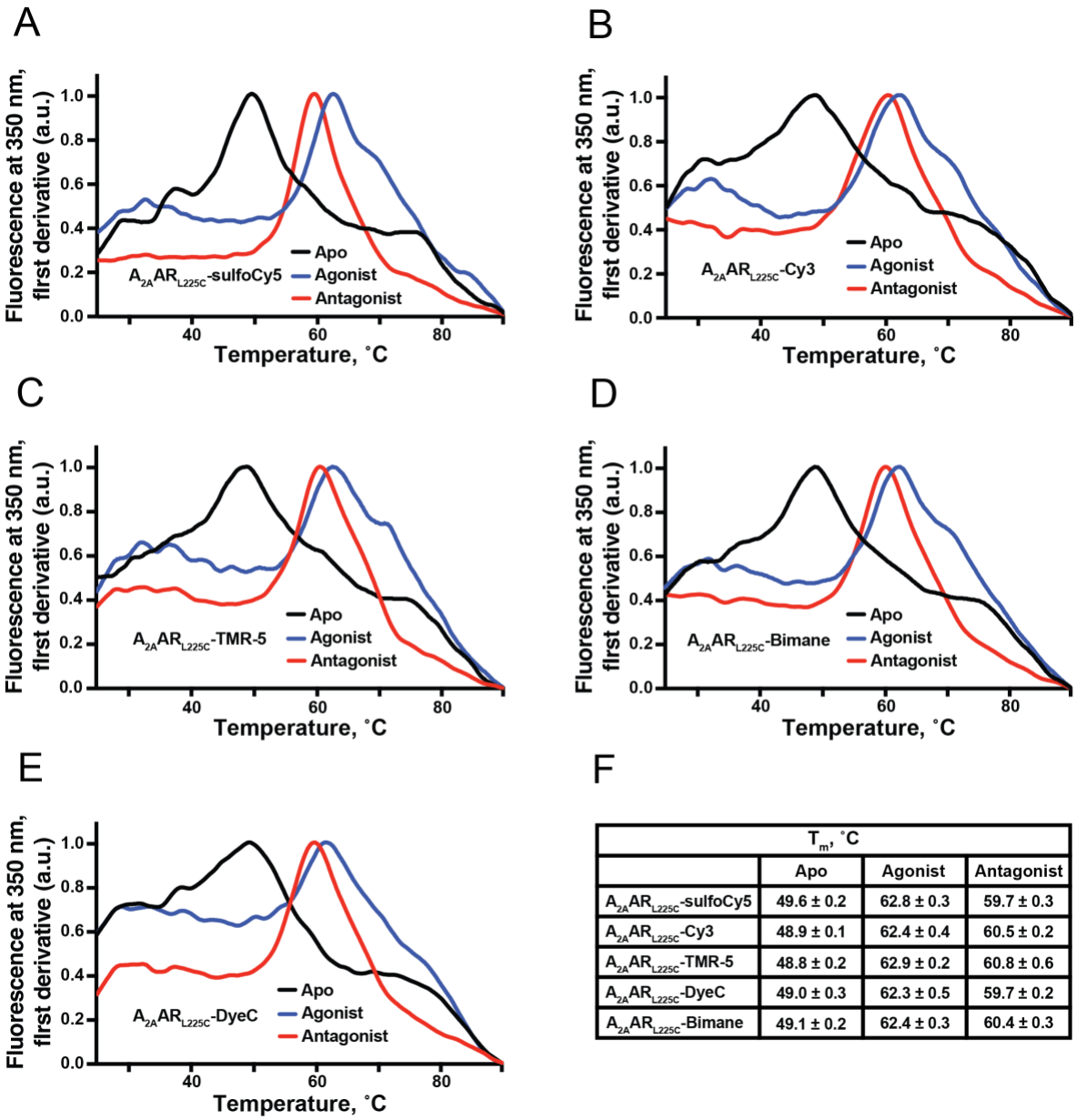

F

	T_m, ˚C		
	Apo	Agonist	Antagonist
$A_{2A}AR_{L225C}$-sulfoCy5	49.6 ± 0.2	62.8 ± 0.3	59.7 ± 0.3
$A_{2A}AR_{L225C}$-Cy3	48.9 ± 0.1	62.4 ± 0.4	60.5 ± 0.2
$A_{2A}AR_{L225C}$-TMR-5	48.8 ± 0.2	62.9 ± 0.2	60.8 ± 0.6
$A_{2A}AR_{L225C}$-DyeC	49.0 ± 0.3	62.3 ± 0.5	59.7 ± 0.2
$A_{2A}AR_{L225C}$-Bimane	49.1 ± 0.2	62.4 ± 0.3	60.4 ± 0.3

Figure S3. Normalized first derivatives of nanoDSF fluorescence curves at 350 nm of $A_{2A}AR_{L225C}$ labeled with various dyes in the apo and ligand-bound states, related to Figure 3. **A-E:** Thermal stability of $A_{2A}AR_{L225C}$ labeled with sulfo-Cy5 (A), Cy3 (B), TMR-5 (C), Bimane (D) or DyeC (E) increases upon addition of agonist (NECA or adenosine), or antagonist ZM241385 compared to its apo state, regardless of the dye used. **F:** Melting temperatures, T_m, were determined as the positions of the maxima of the first derivatives of nanoDSF fluorescence curves (mean ± SD for three technical replicas). Excitation wavelength was 280 nm. All samples were purified from the same batch of cells.

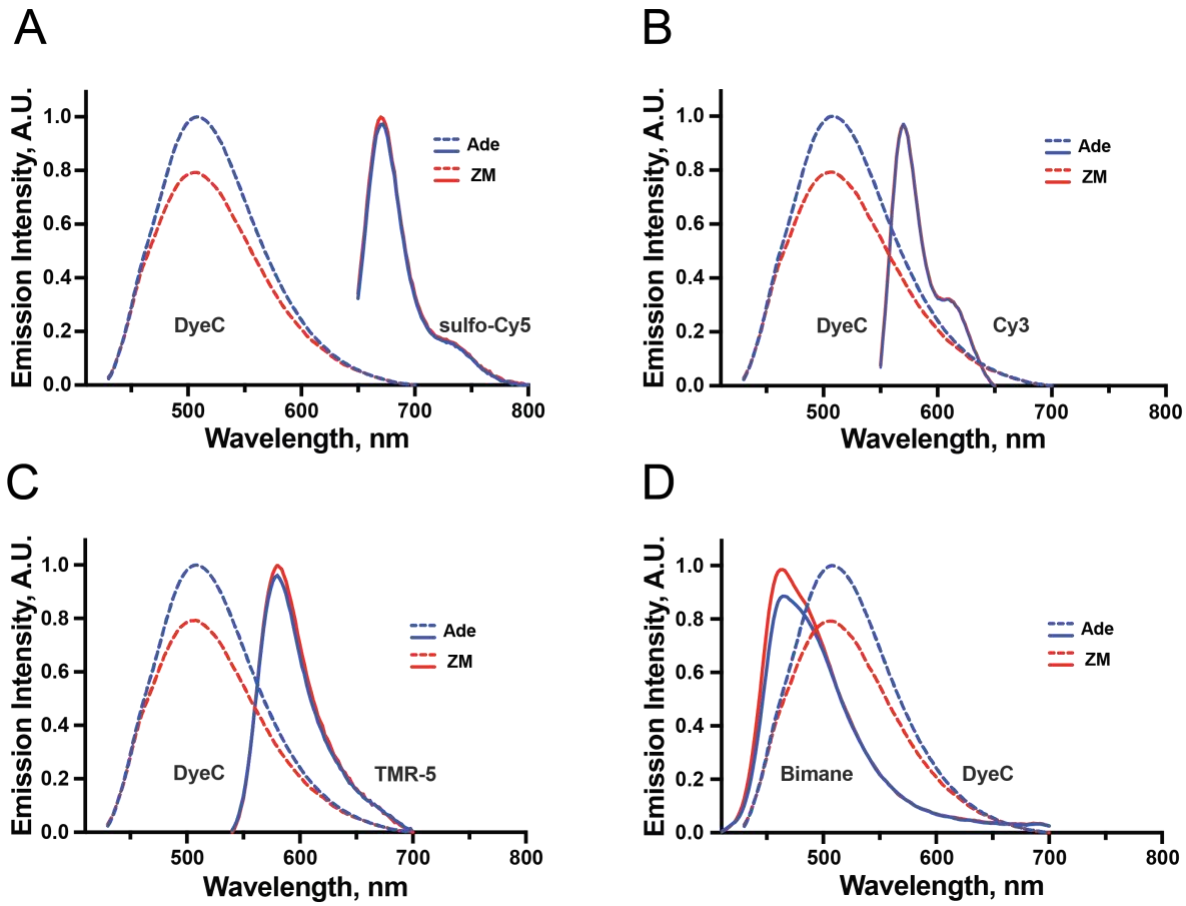

Figure S4. Fluorescence emission spectra of $A_{2A}AR_{L225C}$ labeled with sulfo-Cy5, Cy3, TMR-5, and Bimane and bound with various ligands, related to Figure 3.
Fluorescence emission spectra of sulfo-Cy5 (A), Cy3 (B), and TMR-5 (C) attached to the $A_{2A}AR_{L225C}$ showed no response to the agonist adenosine and antagonist ZM241385. The results suggest that these labels cannot be used as reporters of conformational changes in $A_{2A}AR$. Bimane (D) showed changes in emission spectra, although approximately half as pronounced as those observed with DyeC. DyeC spectra are shown for comparison. All samples were purified from the same batch of cells. Excitation wavelength was 630 nm for **A**, 530 nm for **B**, 520 nm for **C,** and 390 nm for **D**.

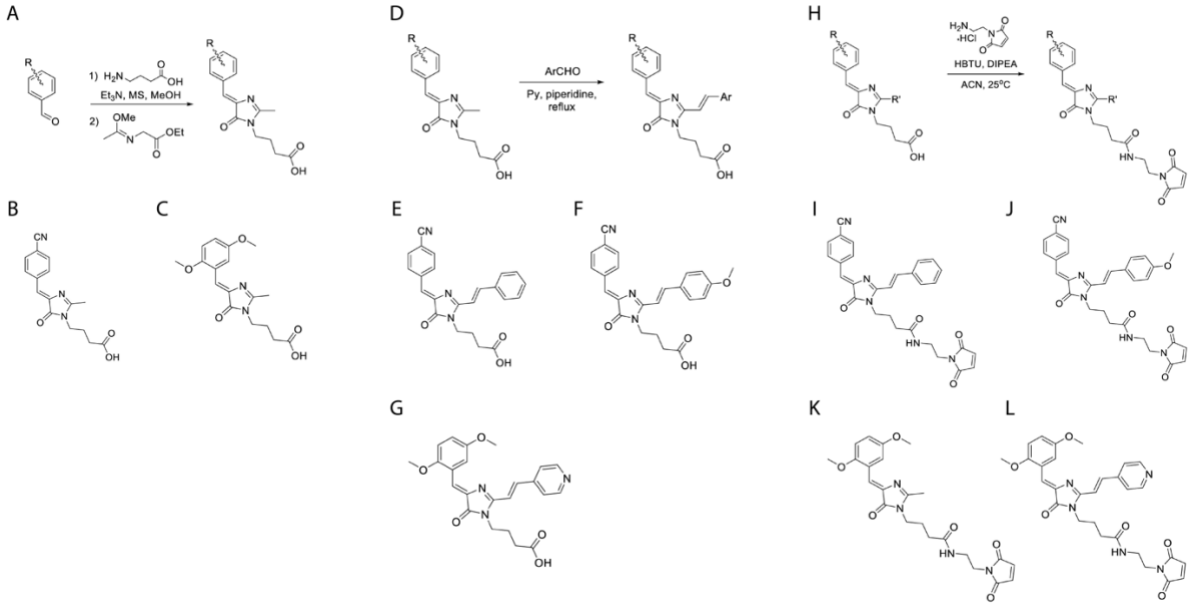

Figure S5. Synthetic procedures of the dyes, related to STAR Methods.
A: Preparation of (Z)-4-(4-benzylidene-2-methyl-5-oxo-4,5-dihydro-1H-imidazol-1-yl)butanoic acids. **B:** (Z)-4-(4-(4-cyanobenzylidene)-2-methyl-5-oxo-4,5-dihydro-1H-imidazol-1-yl)butanoic acid. **C:** DyeC acid. **D:** Preparation of 4-(4-((Z)-benzylidene)-2-((E)-styryl)-5-oxo-4,5-dihydro-1H-imidazol-1-yl)butanoic acids. **E:** DyeA acid. **F:** DyeB acid. G: DyeD acid. **H:** Preparation of 4-(4-((Z)-benzylidene)-5-oxo-4,5-dihydro-1H-imidazol-1-yl)-N-(2-(2,5-dioxo-2,5-dihydro-1H-pyrrol-1-yl)butanamide. **I:** DyeA maleimide. **J:** DyeB maleimide. **K:** DyeC maleimide. **L:** DyeD maleimide.

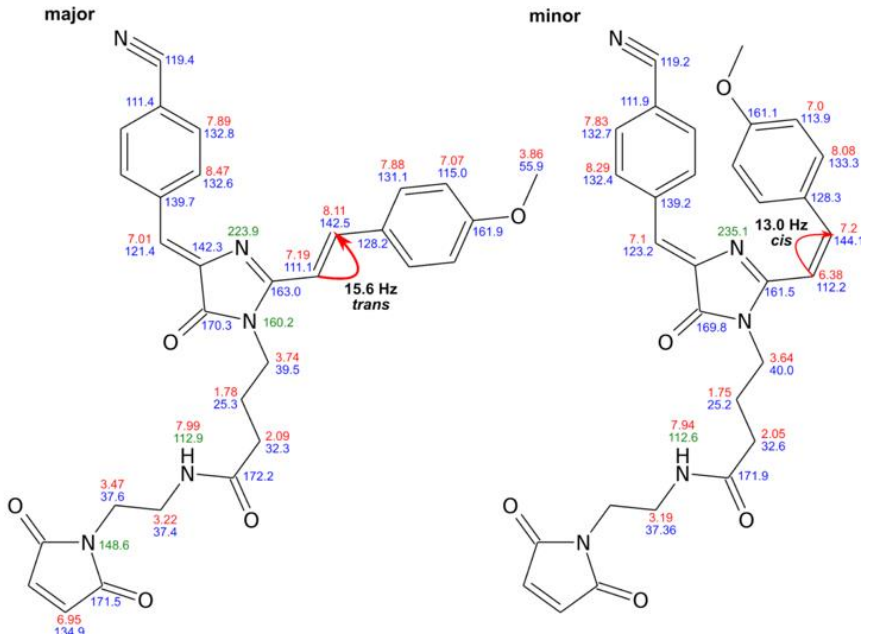

Figure S6. Structures of DyeB maleimide isomers, related to STAR Methods.
Chemical shift assignments are indicated by labels colored in red (^{1}H), blue (^{13}C), and green (^{15}N). The red arrows denote the J-coupling between the double bond protons. Only the different chemical shifts in the minor state are indicated.

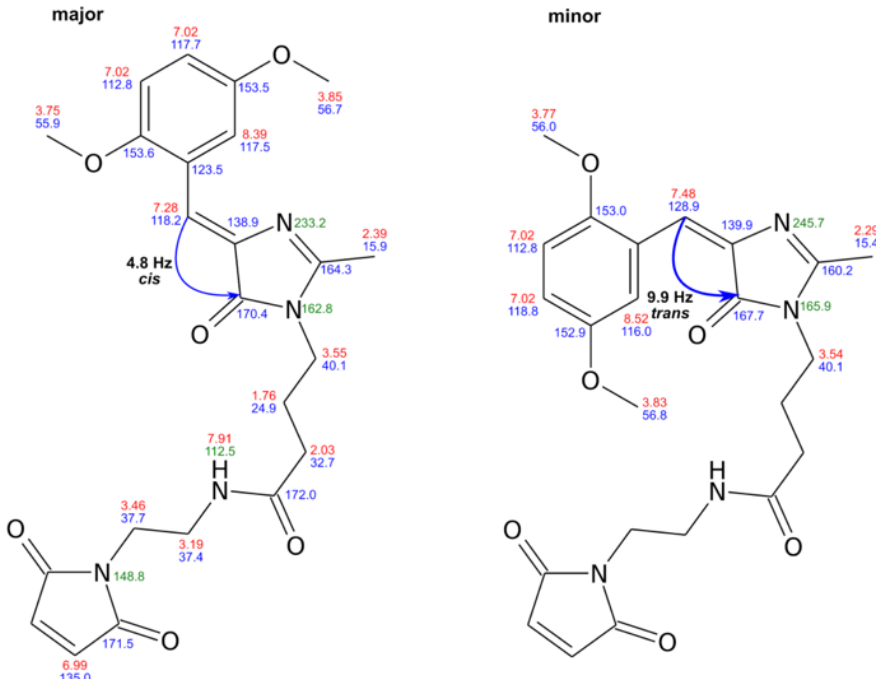

Figure S7. Structures of DyeC maleimide isomers, related to STAR Methods.
Chemical shift assignments are indicated by labels colored in red (^{1}H), blue (^{13}C), and green (^{15}N). The red arrows denote the J-coupling between the double bond protons. Only the different chemical shifts in the minor state are indicated.

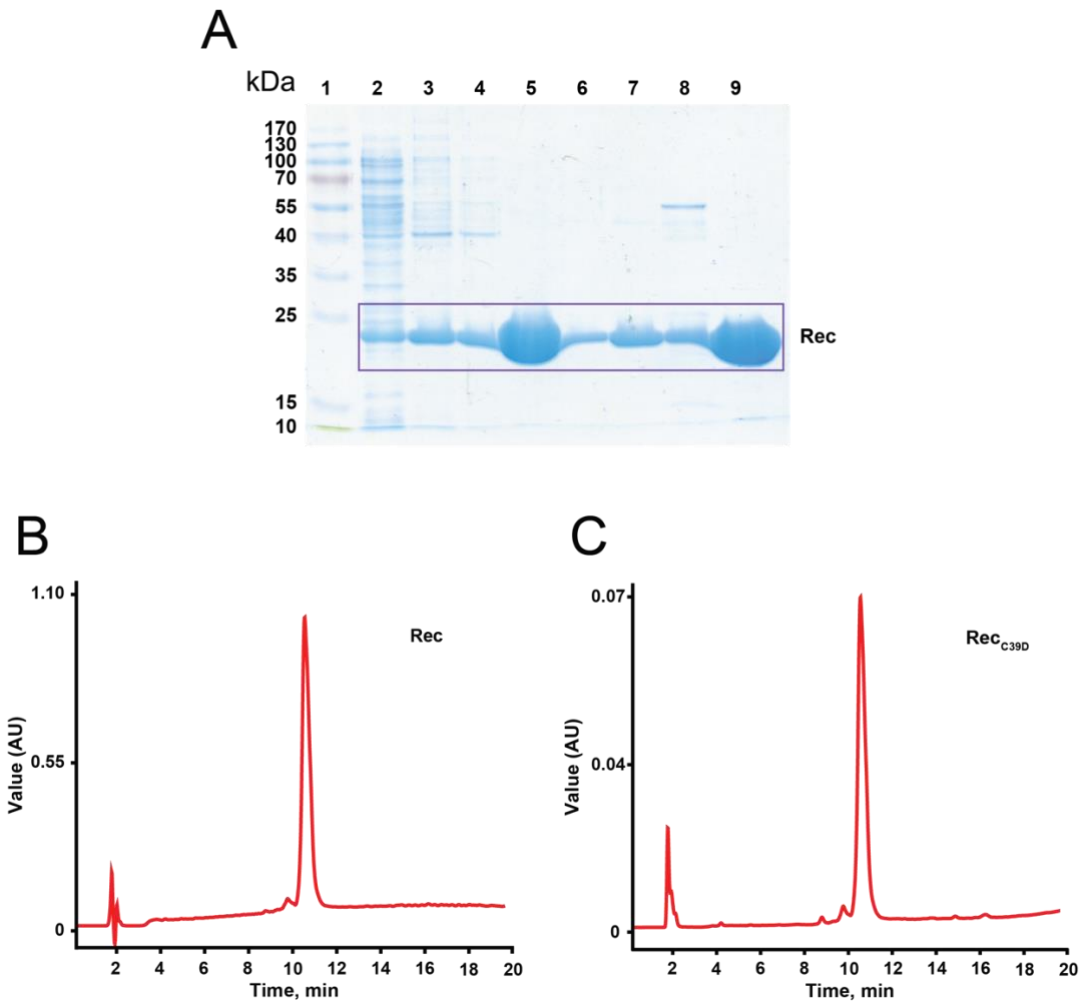

Figure S8. SDS-PAGE (12.5%) and analytical HPLC of Rec and Rec$_{C39D}$, related to STAR Methods. **A:** SDS-PAGE (12.5%) of fractions obtained during purification of Rec and Rec$_{C39D}$. Track 1 – Thermo Scientific™ PageRuler™ Prestained Protein Ladder; Track 2 – Bacterial lysate (Escherichia coli strain BL21-CodonPlus®(DE3)-RIL-X (Agilent), pBB131, pET11d-Rec); Track 3 – Chromatography on Phenyl Sepharose (Cytiva): eluate in 20 mM Tris-HCl, pH=7.5, 1 mM EGTA, 2 mM $MgCl_2$ and 1 mM DTT; Tracks 4-8 – Chromatography on HiTrap Q FF (Cytiva): fractions of gradient 0-1 M NaCl in 20 mM Tris-HCl, pH=7.5, 1 mM DTT; Track 5 – Selected fraction of the myristoylated wild type Rec; Track 9 – Selected fraction of myristoylated Rec$_{C39D}$, purified exactly as described for the wild type Rec. The calculated Rec mass is 23.0 kDa. **B-C:** Analytical HPLC of Rec and Rec$_{C39D}$ in the acetonitrile-water system. Chromatograms of purified Rec **B** and Rec$_{C39D}$ **C** obtained using Breeze QS HPLC System (Waters) equipped with Luna C18 reversed-phase column (Phenomenex) in acetonitrile gradient. Retention time: non-myristoylated Rec/Rec$_{C39D}$ – 9.7 min, myristoylated Rec/Rec$_{C39D}$ – 10.7 min.

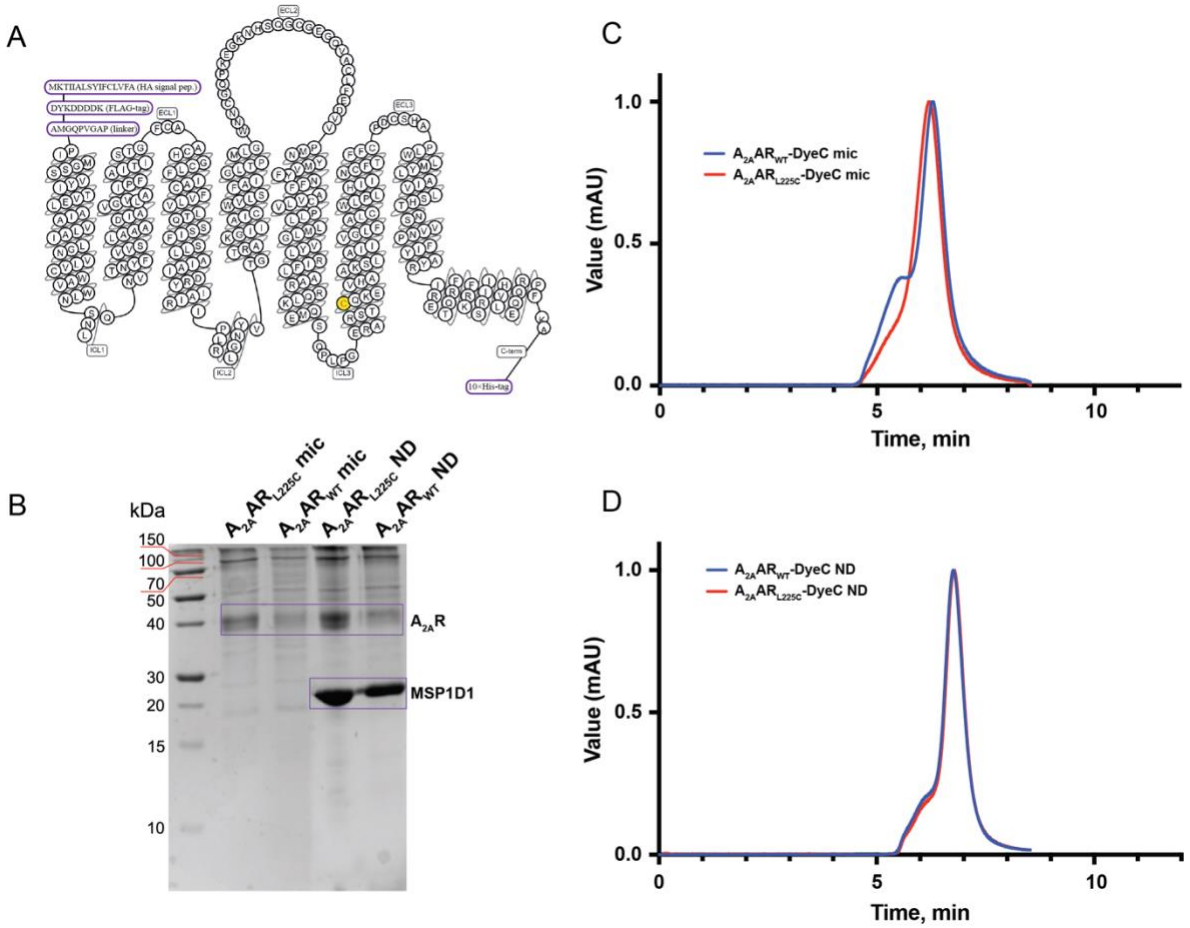

Figure S9. $A_{2A}AR$ constructions used in the work, and their SDS-PAGE and SEC in two different membrane-modeling systems, related to STAR Methods.

A: A snake-plot diagram of the $A_{2A}AR$ construct used in this work. $L225^{6.27}$ residue mutated to cysteine for the labeling is colored in yellow. The snake-plot was drawn using the GPCRdb.org website. **B:** SDS-PAGE of $A_{2A}AR$-DyeC samples. $A_{2A}AR_{WT}$-DyeC and $A_{2A}AR_{L225C}$-DyeC in micelles showed bands around 40 kDa (the calculated $A_{2A}AR$ mass is 39.8 kDa), $A_{2A}AR_{WT}$-DyeC and $A_{2A}AR_{L225C}$-DyeC reconstituted in ND showed two bands: for $A_{2A}AR$ around 40 kDa, and for MSP1D1 around 20 kDa (the calculated MSP1D1 mass is 24.7 kDa). **C:** Normalized analytical SEC of $A_{2A}AR_{L225C}$-DyeC and $A_{2A}AR_{WT}$-DyeC in micelles. **D:** Normalized analytical SEC of $A_{2A}AR_{L225C}$-DyeC and $A_{2A}AR_{WT}$-DyeC in ND. Chromatograms show mostly monomeric protein in both membrane-modeling systems.

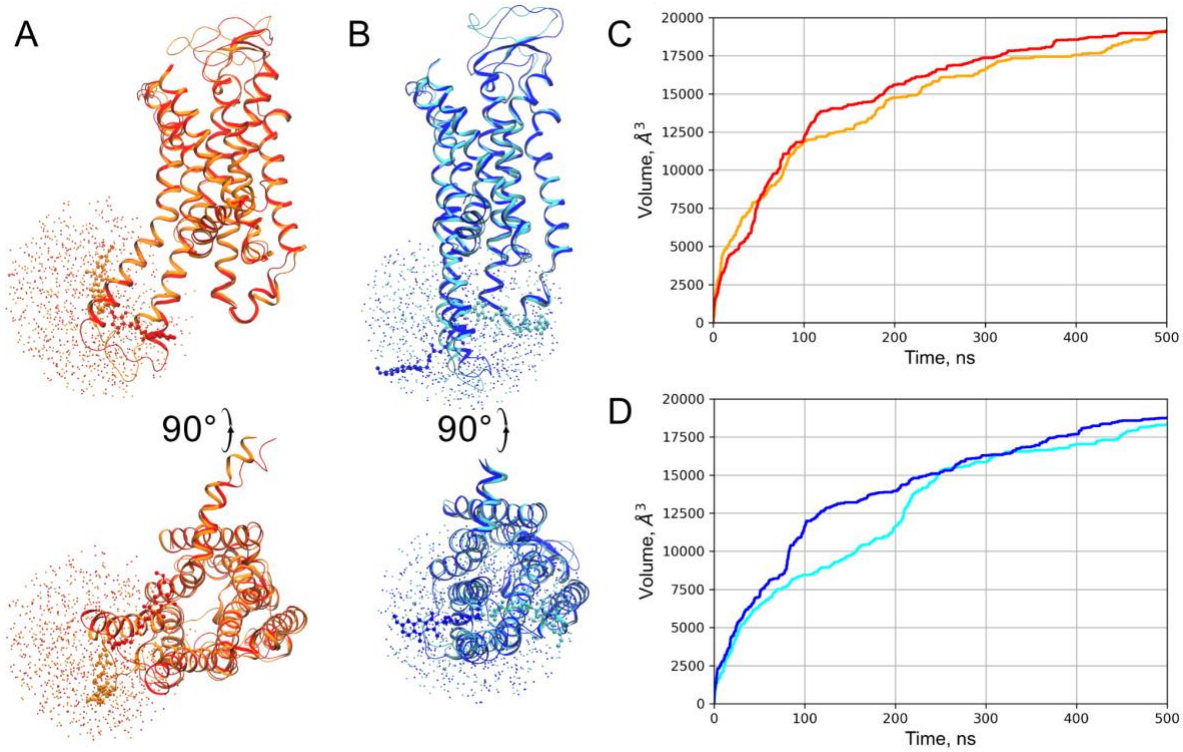

Figure S10. Metadynamics convergence analysis, related to Figure 4.
A-B: Positions of the dimethoxybenzene ring of the DyeC label throughout the metadynamics simulations shown every 1 ns. Each simulation was run for 500 ns. Results for two replicate simulations are shown for each receptor state, in orange and red for the active state, in cyan and blue - for the inactive state. Lipids and water are not shown for clarity. **C-D:** The cumulative volume explored by the fluorescent label plotted as a function of the simulation time for two replicate simulations of the active (panel C) and inactive (panel D) receptor states, colors match those in panels A-B.

Table S1. Solvatochromic properties of maleimide compounds DyeA, DyeB, DyeC, and DyeD, related to Figure 1.

				DyeA			DyeB			DyeC			DyeD		
	Solvent	logP*	Viscosity, mPa·s*	λ_{ABS}, nm	λ_{EM}, nm	FQY, %	λ_{ABS}, nm	λ_{EM}, nm	FQY, %	λ_{ABS}, nm	λ_{EM}, nm	FQY, %	λ_{ABS}, nm	λ_{EM}, nm	FQY, %
1	Water	-1.38	0.9	416	557	0.4	434	575	0.69	~393	~570	0.6	~450	~643	N/D
2	DMSO	-1.35	2.47	431	568	1.9	444	585	2.16	399	502	17.8	461	590	4.1
3	DMF	-1.01	0.8	428	563	1.7	443	580	1.45	395	498	14.1	458	581	6.2
4	MeOH	-0.77	0.54	421	559	1.1	436	575	0.7	398	539	2.9	457	600	0.4
5	ACN	-0.34	0.35	424	564	1.5	437	585	0.82	394	502	7.3	452	583	4.4
6	EtOH	-0.31	1.07	424	555	1.4	440	575	1.11	398	522	4	459	592	1.2
7	Dioxane	-0.27	1.2	425	554	3.4	441	570	1.88	394	477	13.4	452	564	22.4
8	Acetone	-0.24	0.32	425	563	1.7	437	580	0.13	393	485	12.2	450	576	9.2
9	PrOH-1	0.25	2.26	424	559	1.7	N/M	N/M	N/M	398	517	3.8	460	588	2
10	THF	0.46	0.53	427	560	2.3	442	580	1.5	393	475	10.2	451	566	19.8
11	PY	0.65	0.89	431	565	2.6	446	585	2.43	398	489	11.2	463	582	11
12	EtOAc	0.73	0.42	425	554	2.3	438	575	1.37	392	476	10.1	452	564	18.7
13	BuOH	0.88	2.57	N/M	N/M	N/M	442	570	1.66	N/M	N/M	N/M	N/M	N/M	N/M
14	Et_2O	0.89	0.24	424	554	2.6	440	570	1.33	392	466	9.5	446	560	19.4
15	CH_2Cl_2	1.25	0.44	425	560	2.2	441	580	1.28	397	495	4	457	579	7.9
16	Pentanol-1	1.51	3.5	N/M	N/M	N/M	N/M	N/M	N/M	401	507	4.9	N/M	N/M	N/M
17	Toluene	2.73	0.56	429	557	3.8	443	575	1.97	396	475	9.7	456	543	21.4
18	Decanol-1	4.57	10.9	N/M	N/M	N/M	N/M	N/M	N/M	401	491	9.4	N/M	N/M	N/M
19	Undecanol-1	4.72	17.2	N/M	N/M	N/M	446	570	2.92	402	486	10.5	N/M	N/M	N/M
20	Octane	5.18	0.52	426	550	2.3	442	565	1.5	396	458	5.7	449	560	4.1
21	Dodecane	6.1	1.36	~428	~556	N/D	439	565	2.28	396	458	6.3	~451	~567	N/D
22	Pentadecane	7.71	1.95	N/M	N/M	N/M	443	565	2.53	398	462	7.9	N/M	N/M	N/M

* – data from pubchem.ncbi.nlm.nih.gov/compound
N/D – not determined due to low fluorescence
N/M – not measured

Table S2. Integrated Intensity and I_{520}/I_{460} ratios for $A_{2A}AR_{L225C}$-DyeC with various ligands, related to Figure 3.

Ligand	I_{520}/I_{460}	Integrated Intensity
Apo	1.76 ± 0.05 (n = 11)	2.64 ± 0.06 (n = 11)
ZM241385	1.68 ± 0.04 (n = 9)	2.62 ± 0.07 (n = 9)
SCH58261	1.66 ± 0.04 (n = 9)	2.66 ± 0.08 (n = 9)
Adenosine	2.06 ± 0.03 (n = 10)	3.15 ± 0.08 (n = 10)
NECA	1.99 ± 0.05 (n = 15)	3.16 ± 0.03 (n = 15)
HMA	1.42 ± 0.03 (n = 9)	3.03 ± 0.04 (n = 9)

Mean ± SD between repeated experiments are given. For each condition, protein from at least three different purification batches was used, the total numbers of technical repeats are given in brackets.

Table S3. Detection of GPCR structural changes with environmentally sensitive dyes, related to Figure 3.

Dye	Protein	Labelling position	Additional quencher	Mutation	Lipid Modelling System	Max. intensity change, %	Max. λ_{EM} shift, nm	λ_{EM}, nm	λ_{EXC}, nm	ε, M^{-1}. $cm^{-1}\cdot10^3$	Ref.
IANBD	β_2AR	undefined native Cys	-	-	DDM	5	0	523	481	21 [1–3]	[4–6]
FM	β_2AR	$C265^{6.27}$	-	-	DDM	15	N/A	520	490	83 [7]	[8,9]
FM	β_2AR	$C265^{6.27}$	K224-oxyl-NHS	All K to R/$Q224^{5.63}$K	DDM	~23	N/A	520	490	83 [10]	[11]
TMR-5	β_2AR	$C265^{6.27}$	-	-	DDM	~20–~60	N/A	571	541	101 [12]	[13–15]
APM	β_2AR	$C265^{6.27}$ or $C271^{6.33}$	-	C378/406S or C378/406S, $C265^{6.27}$A	DDM	0	<2	625	515	~50 [16]	[17]
Bimane	β_2AR	$C271^{6.33}$	I135W	$C77^{2.48}$V, $C265^{6.27}$/378/406A $C327^{7.54}$S	DDM	~50	0	458	370	5 [18]	[19]
Bimane	β_2AR	$C265^{6.27}$	-	365-trun. or T4 lysozyme fusion	DDM	<26	<8	448	350	5 [18]	[20]
Bimane	β_2AR	$C265^{6.27}$	-	$C77^{2.48}$V, $C327^{7.54}$S, C378/406A	ND	50	15	450	370	5 [18]	[21]
TMR-5	β_2AR	$C265^{6.27}$	-	$C77^{2.48}$V, $C327^{7.54}$S, C378/406A	DDM	15	4	550	515	101 [22]	[23]
Cy3	β_2AR	$C265^{6.27}$	-	$E122^{3.41}$W, res 245-249 removed, $C327^{7.54}$S, $C341^{8.59}$A, 348-trun	ND	~25	N/A	570	532	150	[24]
Cy3	β_2AR	$C327^{7.54}$	-	$E122^{3.41}$W, res 245-249 removed, $C265^{6.27}$A, $C341^{8.59}$A, 348-trun	ND	~25	N/A	570	532	150	[25]
Bimane	GHSR	$C304^{7.34}$ or $C146^{3.55}$	-	$C146^{3.55}$S or $C304^{7.34}$S	ND	~55*	~20	~450	375	5 [18]	[26]
Bimane	Rhodopsin	$C141^{3.56}$ or $C150^{4.39}$ or $C228^{5.63}$ or $C258^{6.41}$ or $C250^{6.33}$	KI	$C140^{3.55}$/$316^{8.53}$/$322^{8.59}$/323S and $K141^{3.56}$C or $E150^{4.39}$C or $F228^{5.63}$C or $V258^{6.41}$C or $V250^{6.33}$C	DDM	~50	~100	460	380	5 [18]	[27]
Bimane	Rhodopsin	$C227^{5.62}$ or $C244^{6.27}$ or $C250^{6.33}$ or $C251^{6.34}$	KI	$C140^{3.55}$/$316^{8.53}$/$322^{8.59}$/323S and $V227^{5.62}$C or $Q244^{6.27}$C or $V258^{6.41}$C or $V250^{6.33}$C	DDM	N/A	12	~460	380	5 [18]	[28]
Bimane	Parapinopsin	$C227^{5.62}$ or $C244^{6.27}$ or $C250^{6.33}$ or $C251^{6.34}$	KI	$V138^{3.53}$F, C140A, $C316^{6.40}$A, C323A and $M227^{5.62}$C or $A244^{6.27}$C or $M258^{6.40}$C or $V250^{6.33}$C	DDM	N/A	7	~465	380	5 [18]	[29]
IAEDANS	A_{2A}AR	$C231^{6.33}$	-	$A231^{6.33}$C	SMALP	50**	0	460	340	6 [30]	[31]
Cy3	A_{2A}AR	$A289^{7.64}$	-	N154Q, $A289^{7.64}$C, 316-trun	ND	~15	N/A	570	532	150	[32]
DyeC	A_{2A}AR	$C225^{6.27}$	-	$L225^{6.27}$C, 316-trun	ND	20	5	515	410	14	this study

* - opposite to other studies, the maximum effect was caused by inverse agonist but not agonist.
** - opposite to other studies, the maximum effect was caused by antagonist but not agonist.
N/A - not available

References

1. Gether, U., Lin, S., and Kobilka, B.K. (1995). Fluorescent Labeling of Purified β2 Adrenergic Receptor: EVIDENCE FOR LIGAND-SPECIFIC CONFORMATIONAL CHANGES (*). J. Biol. Chem. *270*, 28268–28275.

2. Gether, U., Lin, S., Ghanouni, P., Ballesteros, J.A., Weinstein, H., and Kobilka, B.K. (1997). Agonists induce conformational changes in transmembrane domains III and VI of the beta2 adrenoceptor. EMBO J. *16*, 6737–6747.

3. Ghanouni, P., Schambye, H., Seifert, R., Lee, T.W., Rasmussen, S.G.F., Gether, U., and Kobilka, B.K. (2000). The Effect of pH on β2 Adrenoceptor Function: EVIDENCE FOR PROTONATION-DEPENDENT ACTIVATION *. J. Biol. Chem. *275*, 3121–3127.

4. Gether, U., Lin, S., and Kobilka, B.K. (1995). Fluorescent Labeling of Purified β2 Adrenergic Receptor: EVIDENCE FOR LIGAND-SPECIFIC CONFORMATIONAL CHANGES (*). J. Biol. Chem. *270*, 28268–28275.

5. Gether, U., Lin, S., Ghanouni, P., Ballesteros, J.A., Weinstein, H., and Kobilka, B.K. (1997). Agonists induce conformational changes in transmembrane domains III and VI of the beta2 adrenoceptor. EMBO J. *16*, 6737–6747.

6. Ghanouni, P., Schambye, H., Seifert, R., Lee, T.W., Rasmussen, S.G.F., Gether, U., and Kobilka, B.K. (2000). The Effect of pH on β2 Adrenoceptor Function: EVIDENCE FOR PROTONATION-DEPENDENT ACTIVATION *. J. Biol. Chem. *275*, 3121–3127.

7. Ghanouni, P., Steenhuis, J.J., Farrens, D.L., and Kobilka, B.K. (2001). Agonist-induced conformational changes in the G-protein-coupling domain of the beta 2 adrenergic receptor. Proc. Natl. Acad. Sci. U. S. A. *98*, 5997–6002.

8. Ghanouni, P., Steenhuis, J.J., Farrens, D.L., and Kobilka, B.K. (2001). Agonist-induced conformational changes in the G-protein-coupling domain of the beta 2 adrenergic receptor. Proc. Natl. Acad. Sci. U. S. A. *98*, 5997–6002.

9. Ghanouni, P., Gryczynski, Z., Steenhuis, J.J., Lee, T.W., Farrens, D.L., Lakowicz, J.R., and Kobilka, B.K. (2001). Functionally different agonists induce distinct conformations in the G protein coupling domain of the beta 2 adrenergic receptor. J. Biol. Chem. *276*, 24433–24436.

10. Ghanouni, P., Steenhuis, J.J., Farrens, D.L., and Kobilka, B.K. (2001). Agonist-induced conformational changes in the G-protein-coupling domain of the beta 2 adrenergic receptor. Proc. Natl. Acad. Sci. U. S. A. *98*, 5997–6002.

11. Ghanouni, P., Steenhuis, J.J., Farrens, D.L., and Kobilka, B.K. (2001). Agonist-induced conformational changes in the G-protein-coupling domain of the beta 2 adrenergic receptor. Proc. Natl. Acad. Sci. U. S. A. *98*, 5997–6002.

12. Tetramethylrhodamine-5-Maleimide, single isomer https://www.thermofisher.com/order/catalog/product/T6027.

13. Neumann, L., Wohland, T., Whelan, R.J., Zare, R.N., and Kobilka, B.K. (2002). Functional immobilization of a ligand-activated G-protein-coupled receptor. Chembiochem *3*, 993–998.

14. Swaminath, G., Xiang, Y., Lee, T.W., Steenhuis, J., Parnot, C., and Kobilka, B.K. (2004). Sequential Binding of Agonists to the β2 Adrenoceptor: KINETIC EVIDENCE FOR INTERMEDIATE CONFORMATIONAL STATES *. J. Biol. Chem. *279*, 686–691.

15. Swaminath, G., Deupi, X., Lee, T.W., Zhu, W., Thian, F.S., Kobilka, T.S., and Kobilka, B. (2005). Probing the beta2 adrenoceptor binding site with catechol reveals differences in binding and activation by agonists and partial agonists. J. Biol. Chem. *280*, 22165–22171.

16. Cohen, B.E., Pralle, A., Yao, X., Swaminath, G., Gandhi, C.S., Jan, Y.N., Kobilka, B.K., Isacoff, E.Y., and Jan, L.Y. (2005). A fluorescent probe designed for studying protein conformational

change. Proc. Natl. Acad. Sci. U. S. A. *102*, 965–970.

17. Cohen, B.E., Pralle, A., Yao, X., Swaminath, G., Gandhi, C.S., Jan, Y.N., Kobilka, B.K., Isacoff, E.Y., and Jan, L.Y. (2005). A fluorescent probe designed for studying protein conformational change. Proc. Natl. Acad. Sci. U. S. A. *102*, 965–970.

18. Bromobimane Sigma-Aldrich. https://www.sigmaaldrich.com/BE/en/product/sial/b4380.

19. Yao, X., Parnot, C., Deupi, X., Ratnala, V.R.P., Swaminath, G., Farrens, D., and Kobilka, B. (2006). Coupling ligand structure to specific conformational switches in the beta2-adrenoceptor. Nat. Chem. Biol. *2*, 417–422.

20. Rosenbaum, D.M., Cherezov, V., Hanson, M.A., Rasmussen, S.G.F., Thian, F.S., Kobilka, T.S., Choi, H.-J., Yao, X.-J., Weis, W.I., Stevens, R.C., et al. (2007). GPCR engineering yields high-resolution structural insights into beta2-adrenergic receptor function. Science *318*, 1266–1273.

21. Yao, X.J., Vélez Ruiz, G., Whorton, M.R., Rasmussen, S.G.F., DeVree, B.T., Deupi, X., Sunahara, R.K., and Kobilka, B. (2009). The effect of ligand efficacy on the formation and stability of a GPCR-G protein complex. Proc. Natl. Acad. Sci. U. S. A. *106*, 9501–9506.

22. Tetramethylrhodamine-5-Maleimide, single isomer https://www.thermofisher.com/order/catalog/product/T6027.

23. Bockenhauer, S., Fürstenberg, A., Yao, X.J., Kobilka, B.K., and Moerner, W.E. (2011). Conformational dynamics of single G protein-coupled receptors in solution. J. Phys. Chem. B *115*, 13328–13338.

24. Lamichhane, R., Liu, J.J., Pljevaljcic, G., White, K.L., van der Schans, E., Katritch, V., Stevens, R.C., Wüthrich, K., and Millar, D.P. (2015). Single-molecule view of basal activity and activation mechanisms of the G protein-coupled receptor β_2AR. Proc. Natl. Acad. Sci. U. S. A. *112*, 14254–14259.

25. Lamichhane, R., Liu, J.J., White, K.L., Katritch, V., Stevens, R.C., Wüthrich, K., and Millar, D.P. (2020). Biased Signaling of the G-Protein-Coupled Receptor β2AR Is Governed by Conformational Exchange Kinetics. Structure *28*, 371-377.e3.

26. Mary, S., Damian, M., Louet, M., Floquet, N., Fehrentz, J.-A., Marie, J., Martinez, J., and Banères, J.-L. (2012). Ligands and signaling proteins govern the conformational landscape explored by a G protein-coupled receptor. Proc. Natl. Acad. Sci. U. S. A. *109*, 8304–8309.

27. Janz, J.M., and Farrens, D.L. (2004). Rhodopsin activation exposes a key hydrophobic binding site for the transducin alpha-subunit C terminus. J. Biol. Chem. *279*, 29767–29773.

28. Tsukamoto, H., Farrens, D.L., Koyanagi, M., and Terakita, A. (2009). The magnitude of the light-induced conformational change in different rhodopsins correlates with their ability to activate G proteins. J. Biol. Chem. *284*, 20676–20683.

29. Tsukamoto, H., Farrens, D.L., Koyanagi, M., and Terakita, A. (2009). The magnitude of the light-induced conformational change in different rhodopsins correlates with their ability to activate G proteins. J. Biol. Chem. *284*, 20676–20683.

30. Jordanova, R., Radoslavov, G., Fischer, P., Liebau, E., Walter, R.D., Bankov, I., and Boteva, R. (2005). Conformational and functional analysis of the lipid binding protein Ag-NPA-1 from the parasitic nematode Ascaridia galli. FEBS J. *272*, 180–189.

31. Routledge, S.J., Jamshad, M., Little, H.A., Lin, Y.-P., Simms, J., Thakker, A., Spickett, C.M., Bill, R.M., Dafforn, T.R., Poyner, D.R., et al. (2020). Ligand-induced conformational changes in a SMALP-encapsulated GPCR. Biochim. Biophys. Acta Biomembr. *1862*, 183235.

32. Wei, S., Thakur, N., Ray, A.P., Jin, B., Obeng, S., McCurdy, C.R., McMahon, L.R., Gutiérrez-de-Terán, H., Eddy, M.T., and Lamichhane, R. (2022). Slow conformational dynamics of the human A2A adenosine receptor are temporally ordered. Structure *30*, 329-337.e5.